Optical and Magnetooptical Measurements of *N,N′*-Dimethylperylene-3,4,9,10-tetracarboxylic Acid Diimide Thin Films

E. Lifshitz* and A. Kaplan

Department of Chemistry and Solid State Institute, Technion, Haifa, 32000, Israel

E. Ehrenfreund

Department of Physics and Solid State Institute, Technion, Haifa 32000, Israel

D. Meissner

Institut fur Energieverfahrenstechnik, Forschungszentrum Julich GmbH (KFA), Postfach 1913, D-52425, Julich, Germany

Received: August 1, 1997; In Final Form: October 2, 1997

N,N′-Dimethylperylenetetracarboxylic acid diimide (Me-PTCDI) thin films were prepared by vapor deposition technique. The photogeneration and radiative singlet and nonradiative triplet exciton recombination were characterized, utilizing absorption, photoluminescence, and optically detected magnetic resonance (ODMR) spectroscopy. The results suggest the creation of molecular dimers or larger aggregates. The latter effect gives rise to the creation of split singlet exciton states and enhancement of population in the monomer triplet exciton state. The theoretical simulation of the ODMR signal suggests that the dimers are partially oriented with respect to the substrate. They are distributed around the parallel configuration, with a tilt angle of ±36°.

I. Introduction

Perylenetetracarboxylic acid diimide (PTCDI) derivatives can be grown as amorphous or crystalline thin films.[1] These organic films exhibit semiconducting properties with direct bandgap transitions, large visible extinction coefficients, photostability, and low cost of fabrication.[2−9] The latter properties make these semiconductors potentially useful for a number of photoelectronic applications. For example, substituent groups of the organic molecules or external impurities convert these films to either n- or p-type semiconductors from which n/p or organic−metal Schottky junctions can be prepared.[5] The latter can be used in photovoltaic cells[4,5,10] and in photoelectrochemical[11,12] and electrochromic applications.[13] Today, more than 90% of xerographic photoreceptors are made of organic photoconductors.[14,15]

The PTCDI films are prepared by either chemical vapor deposition,[1,8] organic molecular beam deposition,[16,17] plasma polymerization, or spin-coating techniques.[4] Deposition on an amorphous substrate (e.g., indium tin oxide) results in the creation of amorphous or polycrystalline PTCDI films. Deposition on an oriented single crystal of KCl results in the formation of a PTCDI epitaxial structure with a high degree of crystallinity.[16,18] Moreover, epitaxial films of PTCDI with small substituent groups (e.g., Me-PTCDI) crystallize with the molecular plane parallel to the substrate, while the existence of large steric substituents will cause the molecules to stick out from the substrate surface.[18] Schuerlein et al.[17] showed that epitaxial growth of Me-PTCDI on the Cu(100) reactive surface resulted in a crystalline order of the first monolayer, with the molecules parallel to the substrate plane. However, upon initiation of a second layer, island formation appeared, suggesting difficulty in obtaining epitaxial coverage beyond the first monolayer.[17]

The absorption and photoluminescence (PL) spectra of PTCDI derivatives, containing different substituent groups and measured in a similar solution, are essentially identical.[19] This indicates that the spectra are mainly determined by the aromatic core of the molecules (Figure 1), each of which is dominated by $\pi-\pi^*$ or $n-\pi^*$ transitions. In contrast, the optical absorption and PL spectra of the PTCDI bulk or thin films show strong dependence on the substituent groups, relative orientation of the molecules, and crystalline order of the sample.[20]

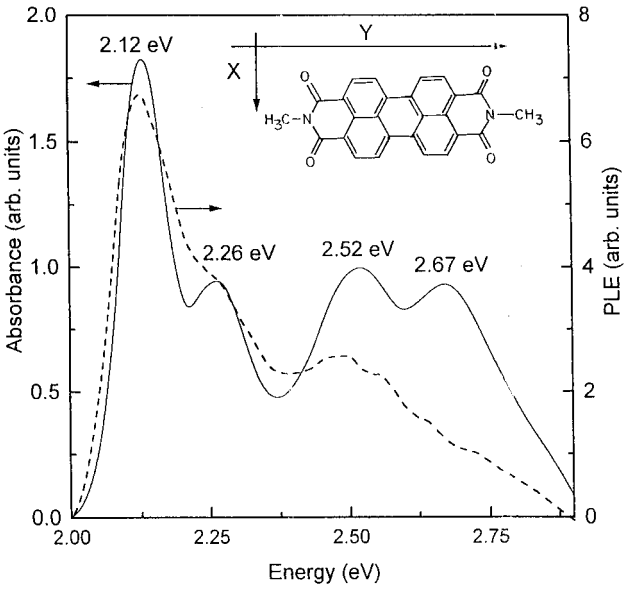

Figure 1. Representative absorption (solid line) and photoluminescence excitation (dashed line) spectra of Me-PTCDI thin films, recorded at 1.4 K. Inset: Molecular structure of the Me-PTCDI molecule.

Photon absorption in organic materials usually leads to the formation of a Frenkel exciton. For example, several authors suggest that the PL spectrum of a Me-PTCDI monolayer film

S1089-5647(97)02505-4 CCC: $15.00
Published on Web 01/16/1998

consists of a monomer exciton emission band, similar to its corresponding solution emission.[21,22] However, thin films of a few monolayers were reported to show a red-shifted emission band, named an excimer exciton. The excimer in solution is defined as a pair of identical molecules, whose interaction is repulsive in the ground state but attractive in the excited state. In thin films, pair of molecules may have a stable ground-state interaction, and thus, their excited-state description is borrowed from the known terminology in solution. The spectrum of bulk α-perylene single crystal exhibits monomer, excimer, and self-trapped exciton emissions. The self-trapped exciton is associated with an intermediate state between the monomer and excimer. Yanagi et al. discussed a possible charge-transfer exciton between two adjacent molecules in a stacked aggregate.[18] They showed that the charge transfer and photoconductivity of amorphous films of Me-PTCDI are less pronounced than those of the corresponding ordered epitaxial film. This is due to the reduced long-range intermolecular interaction and existence of a large amount of grain boundaries in amorphous samples. The above examples indicate that intermolecular interactions and crystallinity play a major role in determining the electronic and optical properties of PTCDI solid samples.

The present article discusses a detailed investigation of *N*,*N*′-dimethyl PTCDI (Me-PTCDI) as a prototype for the study of organic thin films. The research focuses on the study of photogeneration and radiative and nonradiative recombination of singlet and triplet excitons. The above processes were characterized by using absorption, PL, PL excitation (PLE), and optically detected magnetic resonance (ODMR) spectroscopy. The absorption and emission spectra suggest the creation of split exciton states, due to the formation of aggregates. The ODMR measurements confirmed the correlation between the optical properties and crystallinity and enabled one to follow the recombination mechanism.

II. Experimental Section

Me-PTCDI thin films were deposited on a glass substrate by a vapor technique, according to the procedure given in ref 4. The typical thickness of the films was about 300 nm. The absorption, PL, and PLE spectra were recorded by mounting the samples on a vertical probe, immersed in a variable-temperature cryogenic dewar (Janis 12CNDT). The spectra were recorded in the temperature range 1.4−120 K. The samples were excited either by a continuous wave (CW) 2.41-eV (514.5-nm) Ar^+ laser (Coherent, Innova 70) with a power output between 0.5 and 550 mW/cm^2 or with tungsten or xenon arc lamps. The emitted or transmitted light was then dispersed through a holographic grating monochromator (Jobin-Yvon, model THR1000) and detected by an Hamamatsu R666 photomultiplier tube. An Oriel colored glass filter was used in order to eliminate the scattered excitation light.

The ODMR spectra were obtained by measuring the change in luminescence intensity, ΔI_{PL} (or its circular components), induced by a magnetic resonant event at the excited state. Thus, ΔI_{PL} was plotted versus the external magnetic field, H_0 (at a fixed microwave frequency), leading to magnetic resonance-like spectra. The magnetic resonance conditions were achieved by mounting the sample on a special sample probe, containing a homemade TE_{111} microwave cavity, resonating at 10.8 GHz. The microwave source was a synthesized sweeper, amplified by solid-state components, and loop coupled to the cavity via a low-loss cryogenic coaxial cable. The cavity itself was located at the center of a split Helmholtz superconductor magnet (H_0 between 0 and 30 kG), enabling optical access. The whole sample probe was immersed in a cryogenic dewar and cooled to 1.4 K by superfluid helium. The sample was excited by a CW 2.41-eV Ar^+ laser, with a power output of about 0.1−3 W/cm^2. The emitted light was detected by Si PIN photodiode. The microwave power output was amplitude modulated at an audio frequency of 1000 Hz and ΔI_{PL} was detected using a conventional lock-in operation at the microwave modulation frequency. The ODMR signal is detected in either of the following configurations: (a) when the emission wave propagates in the direction, k_{em}, parallel to the external magnetic field (Faraday configuration) or (b) when the emission wave propagates in a direction, k_{em}, perpendicular to H_0 (Voight configuration). A change in the circular polarization component of the luminescence intensity was detected in the Faraday configuration.

III. Results

The absorption spectra of Me-PTCDI thin films were measured in the energy range 2.0−3.4 eV. A representative spectrum, recorded at 1.4 K in the energy range 2.0−2.9 eV, is shown in Figure 1 by the solid line. It consists of an absorption edge, accompanied by four pronounced bands, centered at 2.12, 2.26, 2.52, and 2.67 eV. Moreover, the energy interval between two adjacent bands, starting from the band edge in consecutive order, is 0.14, 0.24, and 0.15 eV, respectively. The absorption above 2.90 eV was truncated in the above presentation. The spectral region above 2.9 eV is associated with the n−π^* transition[19] and will not be taken into consideration in the present document.

The PLE spectra were measured by sweeping the excitation energy between 2.00 and 4.00 eV and detecting the corresponding emission intensity within the range 1.61−1.89 eV. The dashed curve in Figure 1 shows a representative PLE spectrum recorded at 1.4 K and detected at 1.89 eV. The PLE spectra detected at different emission bands are identical. Comparison of the dashed and solid curves in Figure 1 suggests that the excitation process is essentially similar to that of the absorption in the energy range between 2.00 and 2.90 eV. However, the 2.52 and 2.67-eV bands of the PLE are slightly weaker than the corresponding absorption bands. The PLE spectrum contains additional bands, centered at 3.46, 3.61, and 3.82 eV (not shown).

The PL spectra of Me-PTCDI thin films were measured in the temperature range between 2.7 and 140 K. Representative spectra, recorded at three different temperatures, are shown in Figure 2. The PL spectra consist of three bands centered at 1.89 (HE), 1.75 (ME), and 1.61 eV (LE). The energy interval between adjacent emission bands is 0.14 eV.

The ODMR spectra of Me-PTCDI thin films were observed by measuring the change in luminescence intensity of a PL band, due to a magnetic resonance event at the excited state. The ODMR spectrum measured either at the HE, ME, or LE emission band was essentially the same. Moreover, the ODMR spectra, detected in the Voight configuration, showed a spectrum identical to those detected in the Faraday configuration, either with σ^+ or σ^- circular polarization. A typical ODMR spectrum of the above material can be divided into two regions, revolved around $g \approx 2$ and $g \approx 4$, as shown in Figures 3 and 4, respectively. The $g \approx 2$ region (Figure 3) consists of a narrow and intense resonance line, overlapping broad and weak resonance bands. The latter are symmetrically spaced around $g \approx 2$, with mutual separation of about 780 G. The $g \approx 4$ region consists of a single resonance line with fwhm of 14 G. The spectra shown in Figures 3 and 4 are associated with

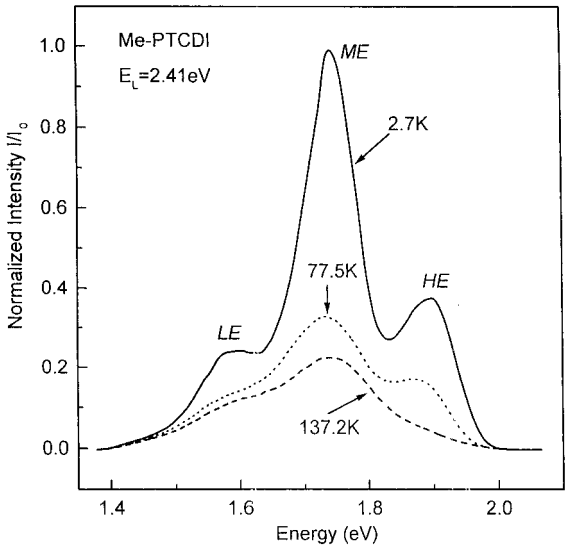

Figure 2. Representative photoluminescence spectra of the Me-PTCDI thin film, recorded at different temperatures, as indicated.

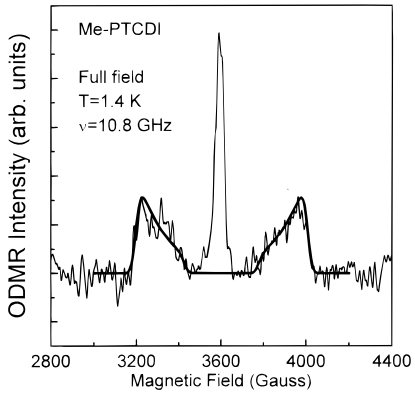

Figure 3. Full-field ODMR spectrum of the Me-PTCDI thin film, recorded at 1.4 K, with a microwave frequency of 10.8 GHz. The bold line corresponds to the simulated triplet exciton resonance.

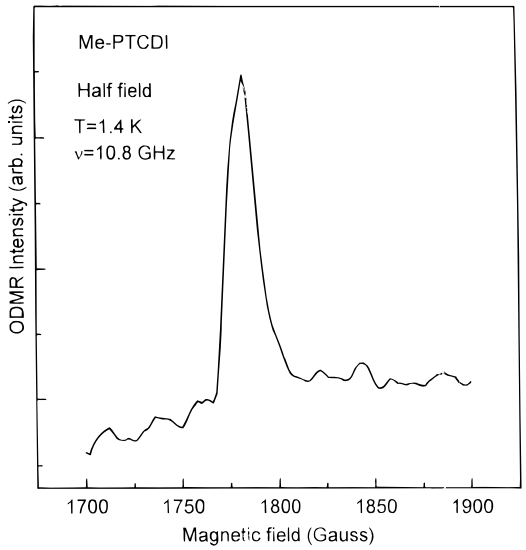

Figure 4. Half-field ODMR spectrum of the Me-PTCDI thin film, recorded at 1.4 K, with a microwave frequency of 10.8 GHz.

enhancement of the luminescence intensity upon magnetic resonance transitions at the excited state, with an absolute change ($\Delta I_{PL}/I_{PL}$) of about 0.1%. The intensity of the entire ODMR spectrum decreases when the audio modulation frequency of the microwave increases above 1000 Hz. It should be noted that the shoulders of the full-field and the single resonance of the half-field ODMR show slight dependence on the relative orientation of the specimen's axis and the direction of the external magnetic field.

IV. Discussion

The absorption and PLE spectra, shown in Figure 1, consist of two progressions, starting at 2.12 and 2.52 eV, respectively. Each subgroup is accompanied by a vibration sideband, separated by 0.14−0.15 eV from its corresponding origin. The latter vibration energy is in close proximity to that of the benzene ring stretching mode.[23] Adachi et al.[19] and Kamura et al.[1] suggest that the band edge transitions correspond to the $\pi-\pi^*$ absorption of the perylene moiety, polarized along the long axis of the planar molecule (see inset in Figure 1). However, the observed progressions in the present case are blue- and red-shifted from the corresponding transition in solution (starting at 2.36 eV[19]). The optical spectra of the corresponding solution have not been recorded, due to solubility problems. However, as mentioned in the Introduction, these transitions are mainly determined by the aromatic moiety, and thus, the previously reported absorption energy[19] should be sufficient for comparison with the present case. The spectral shift of the Me-PTCDI films may indicate a splitting of the excited state due to the creation of aggregates. Kazmaier and Hofmann[20] and several others[24,32] suggested that the energy shift in the optical spectroscopy of PTCDI solids depends on the relative orientation of adjacent molecules within an aggregate, enabling mutual electronic interaction. Kasha et al.[25] showed that the creation of dimers, trimers in organic solids, results in splitting of the singlet exciton state into two states. In the dimer case, each split state is nondegenerate, while in a trimer case one of the states is degenerate. In any event, the split states have different degrees of transition probabilities. The Me-PTCDI film with a thickness much larger than a monolayer, more likely, exhibits short-range ordering, and thus, its molecules may interact with either one or two next neighbors. Then, because of the indistinguishable number of split states depending on the size of the aggregate, the phenomenon will be explained in the following paragraph for the smallest aggregate, the dimer.

The split exciton model is based on the assumption that the intermolecular electron overlap is relatively small. Then, the molecules preserve mainly their electronic structure, while their mutual interaction is considered only as an additional perturbation.[25,26] Thus, the transition energy for the dimer complex is given by the following equation:

$$\Delta E_{\text{dimer}} = \Delta E_{\text{monomer}} + \Delta D \pm \epsilon \qquad (1)$$

where $\Delta E_{\text{monomer}}$ corresponds to the HOMO−LUMO energy difference of the monomer, ΔD corresponds to a variance of the van der Waals interaction in the ground and excited state, and $\pm\epsilon$ corresponds to an exchange of excitation energy between the molecules. The last term can be approximated by a point-dipole−point-dipole interaction, leading to splitting of the exciton electronic state. The value of the exciton splitting term depends on the mutual orientation of the molecules within the dimer and is given by the following equation:

$$\Delta\epsilon = 2|M|^2/r^3(\cos\alpha + 3\cos^2\theta) \qquad (2)$$

where M is the transition moment for the singlet−singlet absorption in the monomer, r is the line connecting the centers of the molecular units, α is the angle between the transition dipoles of the monomers, and θ is the angle made between a

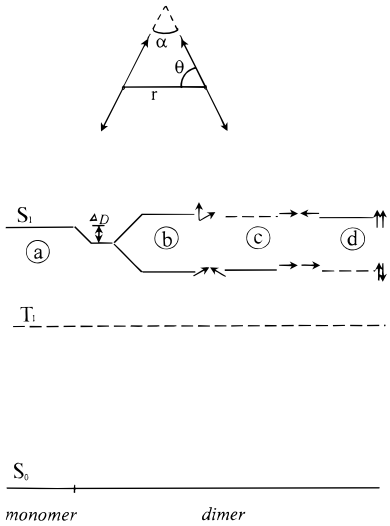

Figure 5. Schematic diagram of monomer and dimer exciton electronic levels. The arrows correspond to the transition dipole moments. The solid lines correspond to optically allowed states, while the dashed lines represent forbidden states. The geometrical factors α, θ, and r are explained in the text. Diagram a represent the monomer exciton electronic structure. Diagram b corresponds to the exciton electronic structure of an oblique dimer. Diagrams c and d correspond to a dimer structure with coplanar arrangement, with the molecules in head-to-tail and parallel configurations, respectively.

dipole of a monomer and r. The geometrical factors are presented at the top of Figure 5, where the arrors correspond to the transition dipoles. The energy diagram in Figure 5 represents the electronic energy levels of a monomer and dimers, emphasizing the splitting of the singlet excited state in the dimer into two states. The optically allowed states are shown by the solid lines, while the forbidden states are given by the dashed lines. It should be emphasized that the triplet state, more probably, is not split by the formation of aggregates. This can be due to the relatively slow and weak exchange of triplet excitation between next neighbor molecules. This assumption is generalized in ref 25 for several cases of molecular aggregates. Hence, the triplet state of dimer and monomer will be indistinguishable and is presented by the dashed line in Figure 5. Figure 5a corresponds to the monomer electronic structure, including the van der Waals contribution, ΔD. Figure 5b corresponds to a geometry in which the monomers are oriented with an oblique angle, α, with respect to each other. The dipole−phase relation indicates that transitions into both states are allowed. Figure 5c corresponds to a case in which $\alpha = 0$ and $\theta = 0°$, when the molecules are arranged in a head-to-tail configuration. The latter geometry leads to an energy scheme in which the lower state is optically allowed and, thus, results in a red shift of the singlet−singlet absorption band. Figure 5d corresponds to a case in which the molecules are coplanar ($\alpha = 0$) with $\theta = 90°$. In this configuration the molecules are precisely parallel to each other, enabling efficient overlap of the transition dipoles. The latter give rise to a preferred transition into the upper state, causing a blue shift of the singlet−singlet absorption bands.

The exciton splitting, observed in the absorption and PLE spectra of Me-PTCDI thin films (Figure 1), is estimated to be $\Delta\epsilon = 0.4$ eV. The transition dipole moment of the monomer was evaluated as $M = 4.7$ eV$^{1/2}$ Å$^{3/2}$, on the basis of the absorption energy and oscillator strength, reported in ref 19. Thereupon, the distance between the centers of the molecules within the dimer was calculated using eq 2. For example, in the head-to-tail configuration, $\theta = 0°$, $\alpha = 0°$, and thus, $r = 7.7$ Å. On other hand, for $\theta = 90°$ and $\alpha = 0°$, $r = 4.85$ Å.

The above representative calculations consider coplanar geometry with longitudinal displacement of the molecules, one with respect to the other, within the dimer. Klebe et al.[27] developed an empirical equation, predicting the absorption wavelength of an aggregate, including longitudinal (l) and transverse (t) displacements, as given in eq 3. Since the dimer intermolecular spacing, d, was reported to be nearly the same ($d = 3.5$ Å) for numerous PTCDI derivatives, the empirical equation includes the displacement distances alone:

$$\lambda_{max} = 9.718t^2 - 82.009t - 21.888l + 735.329 \quad (3)$$

It should be noted that $r^2 = d^2 + l^2 + t^2$. Examination of the 2.12−eV absorption band in Figure 1 leads to a maximal transverse displacement of 4.6 Å (at $l = 0$), maximal longitudinal displacement of 6 Å (at $t = 0$), and $r = 8.3$ Å. The latter value may correspond to the head-to-tail configuration and is in close proximity to that derived from the exciton splitting model. Moreover, the transverse and longitudinal displacements are in close agreement with the dimensions of the Me-PTCDI monomer.

Considering the general description given above, the appearance of two absorption and excitation progressions could be due either to the existence of oblique dimers or to the existence of a mixture of coplanar dimers with different mutual displacement. Alternatively, distortions in the aggregate geometry can lead to a small probability of transition associated with the forbidden split state, within a single coplanar configuration.

Previously reported PL spectra of PTCDI in solution show a typical progression in the green part of the spectral region, associated with the monomer moiety.[21,32] On the contrary, the reported PL spectra, recorded on α-perylene single crystals[28−30] or thin films of PTCDI,[31] showed a featureless band in the red spectral region, suggesting the recombination of a so-called excimer state.[32] Comparison of the PL spectra presented in Figure 2 with the indicated reports reflects the absence of a monomer structure. Moreover, the appearance of a resolved progression in the red spectral region excludes the existence of an excimer and further supports an emission from split exciton states of dimers or larger aggregates. The PL spectrum was simulated theoretically, utilizing the following equation:[33]

$$I_{0-n} \propto \sum_{n=0}^{\infty} \frac{S^n}{n!} \exp\left\{\frac{-\ln 2[E - (E_{0-0} - nh\nu)]^2}{\Gamma^2}\right\} \quad (4)$$

where I_{0-n} is the intensity of the vibronic line n, Γ is the full width at half-maximum, and $h\nu$ is the vibration frequency. S is the Huang Ryss factor,[34] reflecting the displacement of the excited-state potential, with respect to that of the ground state. The PL spectrum was fitted to an overlap of two progressions, with an electronically and a vibronically (electronic and vibration mixing) allowed origin, at $E_{low(0-0)}$ and $E_{high(0-0)}$, respectively. Representative simulation of the PL spectrum is shown in Figure 6. The solid curve corresponds to the experimental spectrum, recorded at 1.4 K, while the dotted and dashed curves correspond to the simulated progressions. The latter originate at $E_{low(0-0)} = 1.74$ eV ($S_{low} = 0.39$), $E_{high(0-0)} = 2.05$ eV ($S_{high} = 0.30$) and coupled to a vibrational mode of 0.157 eV. It should be noted that the $E_{high(0-0)}$ is not pronounced in the spectrum, and instead, the $E_{high(0-1)}$ transition is the leading component of this progression. The progressions' origin is Stokes-shifted from the corresponding absorption edge by 0.38−0.47 eV. This

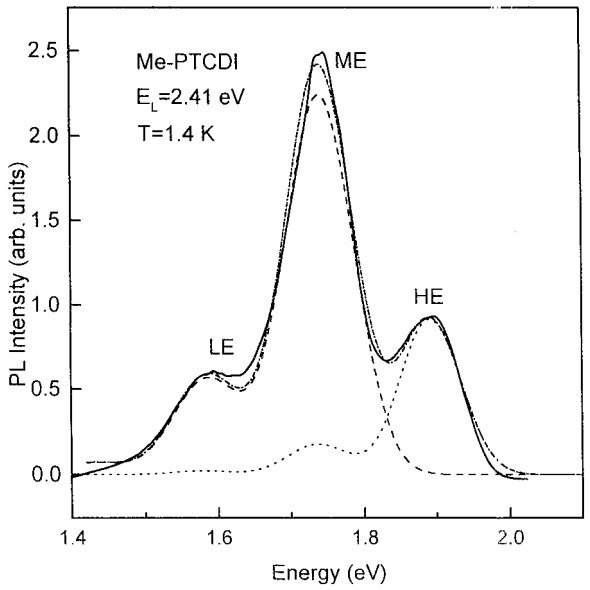

Figure 6. Representative simulation of the photoluminescence spectrum at 1.4 K. The solid line corresponds to the experimental data. The dotted and dashed lines are associated with simulated progressions, setting on at $E_{0-0(\text{high})} = 2.05$ eV and $E_{0-0(\text{low})} = 1.74$ eV, respectively. The dot−dashed line corresponds to the sum of the latter progressions.

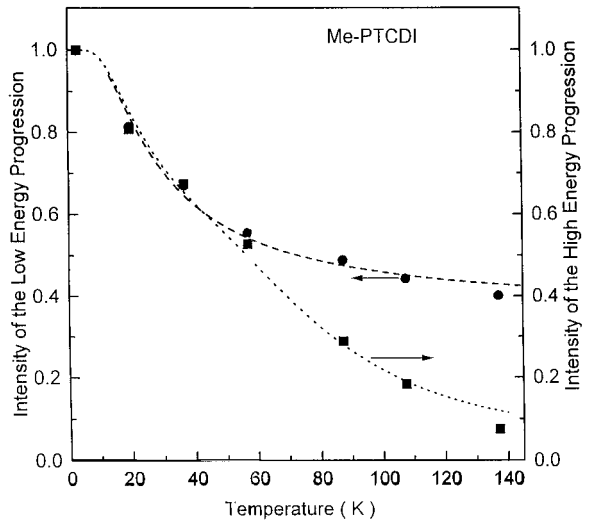

Figure 7. Plot of the normalized and integrated intensity of the low and high simulated PL progressions versus temperature.

large shift can be due to the localization and the large binding energy of the exciton complex in organic thin films. The electronically allowed progression may be associated with the upper split exciton state, while the vibronically allowed progression corresponds to the lower state. Thus, the components of the emission spectrum may favor the existence of dimers with coplanar configuration (diagram c or d in Figure 5).

The normalized and integrated intensity of the simulated progressions, composing the PL spectrum, is plotted versus temperature, in Figure 7. The circles and squares in the figure correspond to the low- and high-energy progressions, respectively. The temperature dependence of the PL originates from the competition among the radiative and several nonradiative recombination processes. This competition can be described by classical rate equations, assuming that the radiative process is independent, while the nonradiative processes depend on the temperature. Similar treatment has been given in ref 35. On the basis of these arguments the temperature dependence, shown in Figure 7, has been simulated by the following equation and is shown by the dashed line in the figure:

$$I(T) \propto \frac{1}{1 + B_1 \exp\left(\frac{-\Delta E_1}{kT}\right) + B_2 \exp\left(\frac{-\Delta E_2}{kT}\right)} \quad (5)$$

The best fit parameters, for the low-energy progression, are $B_1 = 1.84$, $\Delta E_1 = 3.9$ meV, and $B_2 = 0$. The parameters for the high-energy progression are $B_1 = 1.84$, $\Delta E_1 = 3.9$ meV, $B_2 = 70$, and $\Delta E_2 = 28$ meV. Thus, the low-energy progression is quenched by a single thermalization process with an activation energy of 3.9 meV. The quenching of the high-energy progression is dominated by coupling to a low-frequency mode (3.9 meV) up to 50 K, which is exchanged by another coupling mechanism, with higher frequency mode (28 meV), above 50 K. The low-frequency mode may be associated with sliding motion of one molecule with respect to the other. Such a libration motion, with low acoustic phonon frequency, was reported in the past for layered semiconductors.[36] In a similar manner, a low activation energy of about 5 meV was report in poly(paraphenylvinylene) (PPV).[37]

The ODMR spectra of the Me-PTCDI thin films showed identical shape when detected at the HE, ME, and LE luminescence bands, further supporting the existence of one or two progressions, as derived from the PL spectra. The observed spectra showed slight anisotropic behavior regarding the orientation of the films, with respect to the external magnetic field. This reveals partial orientation of the aggregates within the film (vide infra). The $g \approx 2.0$ region consists of a sharp resonance, typical of an unpaired electron, such as a free radical or polaron. The side shoulders resemble a typical powder pattern of a triplet exciton, associated with the $\Delta M_s = \pm 1$ transitions. Moreover, the $g \approx 4.0$ resonance corresponds to the triplet $\Delta M_s = \pm 2$ transition.

The observation of a triplet resonance with unresolved hyperfine structure suggests that the spin system of Me-PTCDI is mainly influenced by the Zeeman (g_{eff}) and dipole−dipole interaction (D, E). As will be shown below, the triplet exciton considered in the present case has an extremely small effective radius. In such a case, the isotropic exchange interaction is assumed to be extremely large, causing the spin singlet to lie at much higher energy than the corresponding triplet spin states. Then, the resonance transition and relaxation to the ground state may take place from the triplet spin manifold alone, and the exchange interaction contribution may be ignored.[38−40] Thus, the spin system can be described by the following spin Hamiltonian:

$$\mathrm{H} = \beta S g_{\text{eff}} B + D(S_z^2 - {}^1/_3 S^2) + E(S_x^2 - S_y^2) \quad (6)$$

$$g_{\text{eff}}^2 = g_{\parallel}^2 \cos^2\theta + g_{\perp}^2 \sin^2\theta \quad (7)$$

where S_i correspond to the spin component and B corresponds to the strength of the external magnetic field components. Considering the planar structure and the difference between the long (y) and short (x) axis of the PTCDI monomer, it is reasonable to assume that the g principal axis has an axial symmetry, with $g_{\parallel}$ coinciding with the y molecular axis. In a manner similar to other conjugated molecular crystals (e.g., naphthalene), the dipole−dipole interaction of the Me-PTCDI is assumed to be nonaxial symmetric ($E \neq 0$), with the z principal axis perpendicular to the molecular plane. The simulation of the triplet exciton resonance excluded the existence of either random orientation or perfect alignment of the dimers within the films. However, consideration of partial orientation

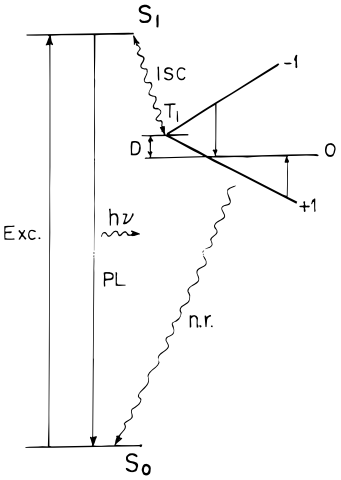

Figure 8. Schematic diagram of the electronic and spin exciton levels. The ±1 and 0 notations correspond to the spin quantum numbers of the triplet exciton. D is associated with the zero field splitting. The S_1 state is associated with the E″ or E′ split exciton level.

led to a good agreement with the experimental data. The bold line in Figure 5 represents a simulation in which the dimers were considered to be distributed around parallel orientation with respect to the substrate, with a tilt angle of ±36°. More explicit details of the magnetic resonance simulations will be given elsewhere. The described simulation considered the following magnetic resonance parameters: $g_{\text{eff}} = 2.003$, $D/g_{\text{eff}}\beta = 810$ G, and $E/g_{\text{eff}}\beta = 80$ G. The zero-field parameter, D, yields a rough estimation of the triplet exciton radius, on the basis of the following relation:

$$R \cong \left(\frac{3}{4}\frac{g_{\text{eff}}{}^2\beta^2}{D}\right)^{1/3} \tag{8}$$

Considering $g_{\text{eff}} \approx 2.0$, the calculated R is 3 Å. This radius is slightly smaller than the diameter of the benzene ring. A small size of a triplet exciton was observed before in other conjugated organic semiconductors (e.g., PPV).[41] The latter may indicate that the exciton is localized within a monomer, and the latter is consistent with the assumption given above and shown in Figure 5, about the monomeric character of the triplet state.

The pronounced triplet effect in the ODMR spectrum is not surprising. It is well-known that split excitons in dimers show enhancement of the intersystem crossing into the triplet state. As shown in the diagrams of Figure 5, one exciton state is usually more allowed than the other. Thus, the so-called forbidden state has a longer lifetime, providing the means for intersystem crossing into the monomer triplet state. Then, the triplet relaxation can be either radiative or nonradiative. It should be noted that the PL spectra of the Me-PTCDI thin films correspond to the fluorescence phenomenon and do not include a phosphorescence contribution. The latter conclusion is based on the emission decay measurements (not shown), indicating an excited-state lifetime on the order of a nanosecond. Consequently, the ODMR phenomenon in the present case is associated with a nonradiative triplet state. Still, the spectra showed enhancement of the luminescence intensity, due to magnetic resonance event in the excited state among the triplet sublevels. Such an enhancement can take place when the radiative and nonradiative routes are coupled via the ground state, as shown schematically in Figure 8. Nonradiative relaxation from either one of the triplet sublevels enhances the ground-state population, further increases the singlet−singlet excitation, and eventually increases the total luminescence intensity.

V. Summary

The absorption, PL, and PLE investigations, described above, suggest the creation of split exciton states due to the formation of dimers or larger aggregates within the solid thin films with a typical thickness of about 300 nm. The molecular units within an aggregate have, more likely, a coplanar configuration. The ODMR results suggest that the creation of aggregates enhances the intersystem crossing into a monomer triplet state. According to the ODMR investigation, the aggregates are partially oriented within the thin film. The overall optical and magnetooptical measurements suggest strong localization of the exciton inside a monomer or a small aggregate.

Acknowledgment. The authors thank Prof. T. Schaafsma and Prof. S. Speiser for stimulating discussions. This work was partly supported by the Israel Science Foundation, contract No. 335/94. A.K. expresses his gratitude to the Ministry of Science for the student fellowship.

References and Notes

(1) Kamura, Y.; Shirotani, I.; Ohno, K.; Inokuchi, H. *Bull. Chem. Soc. Jpn.* **1976**, *49* (2), 418.
(2) Gasyna, I.; Kabayashi, N.; Stillman, M. J. *J. Chem. Soc., Dalton Trans.* **1989**, 2397.
(3) Tsutsui, T.; Nakashima, T.; Fujita, Y.; Saito, J. *Synth. Met.* **1995**, *7*, 1281.
(4) Wohrle, D.; Meissner, D. *Adv. Mater.* **1991**, *3*, 129.
(5) Wohrle, D.; Kreienhoop, L.; Schnupfeil, G.; Elbe, J.; Tannigkeit, B.; Hiller, S.; Schlettwein, D. *J. Mater. Chem.* **1995**, *5*, 1819 and references within.
(6) Nevin, W. A.; Chamberlain, G. A. *J. Chem. Soc., Faraday Trans.* **1989**, *85* (2), 1729.
(7) Nevin, W. A.; Chamverlain, G. A. *J. Chem. Soc., Faraday Trans.* **1989**, *85* (2), 1747.
(8) Gregg, B. A.; Fox, M. A.; Bard, A. J. *J. Phys. Chem.* **1990**, *94*, 1586.
(9) Antohe, S. *Phys. Status Solidi* **1993**, *136*, 401.
(10) Zweibel, K. *Am. Sci.* **1993**, *81*, 361.
(11) Schlettwein, D.; Kaneko, M.; Yamada, A.; Wohrle, D.; Jaeger, N. I. *J. Phys. Chem.* **1991**, *95*, 1748.
(12) Danziger, J.; Dodelet, J. P.; Lee, P.; Nebesny, K. W.; Armstrong, N. R. *Chem. Mater.* **1991**, *3*, 821.
(13) Schlettwein, D.; Wohrle, D.; Jaeger, N. I. *J. Electrochem. Soc.* **1989**, *136*, 2882.
(14) Law, K. Y. *Chem. Rev.* **1993**, *93*, 449.
(15) Loutfy, R. O.; Hsiao, C. K; Hor, A. M.; DiPaola-Baranyl, G. *J. Imaging Sci.* **1985**, *29*, 148.
(16) Fuchigami, H.; Tanimura, S.; Uehara, Y.; Kurata, T.; Tsunoda, S. *Jpn. J. Appl. Phys.* **1995**, *34*, 3852.
(17) Schuerlein, J.; Schmidt, A.; Lee, P. A.; Nebesny, K. W. *Jpn. J. Appl. Phys.* **1995**, *34*, 3837.
(18) Yanagi, H.; Toda, Y.; Noguchi, T. *Jpn. J. Appl. Phys.* **1995**, *34*, 3808.
(19) Adachi, M.; Murata, Y.; Nakamura, S. *J. Phys. Chem.* **1995**, *99*, 14240.
(20) Kazmaier, P. M.; Hoffman, R. *J. Am. Chem. Soc.* **1994**, *116*, 9684.
(21) Vitukhovsky, A. G.; Sluch, M. I.; Warren, J. G.; Petty, M. C. *Chem. Phys. Lett.* **1990**, *173*, 425.
(22) Puech, K.; Frob, H.; Hoffman, M.; Leo, K. *Opt. Lett.* **1996**, *21*, 1606.
(23) Akers, K.; Aroca, R.; Hor, A.-M.; Loutfy, R. *J. Phys. Chem.* **1987**, *91*, 2954.
(24) Rohatgi, K. K.; Mukhopadhay, A. K. *J. Phys. Chem.* **1972**, *76*, 3970.
(25) Kasha, M.; Rawls, H. R.; El-Bayoumi, A. *Pure Appl. Chem.* **1965**, *11*, 371.
(26) Muto, J. *J. Phys. Chem.* **1976**, *80*, 1342.
(27) Klebe, G.; Graser, F.; Hadicke, E.; Berndt, J. *Acta Crystallogr. B* **1989**, *45*, 69.

(28) Hochstrasser, R. M.; Nyi, C. A. *J. Chem. Phys.* **1980**, *72*, 2591.
(29) Matsui, A. H. *Pure Appl. Chem.* **1995**, *67*, 429.
(30) Tamai, N.; Porter, C. F.; Masuhara, H. *Chem. Phys. Lett.* **1993**, *211*, 364.
(31) Johnson, E.; Aroca, R.; Nagao, Y. *J. Phys Chem.* **1991**, *95*, 8840.
(32) Burgdorff, C.; Lohmannsroben, H.-G.; Reisfield, R. *Chem. Phys. Lett.* **1992**, *197*, 358.
(33) Herzberg, G. *Spectra of diatomic molecules*; Van Nostrand: Princeton, 1950; p 199.
(34) Huang, K.; Rhys, A. *Proc. R. Soc. London* **1950**, *A204*, 403.
(35) Klick, C. C.; Schulman, J. H. *Solid State Physics*, Vol. 5; Academic Press: New York, 1957.
(36) Skolnik, M. S.; Dimberg, D. *Phys. Rev. B* **1978**, *18*, 7080.
(37) Bradley, D. C.; Friend, R. *J. Phys.: Condens. Matter* **1989**, *1*, 3671.
(38) Davies, J. J.; Cox, R. T.; Nichols, J. E. *Phys. Rev. B* **1984**, *30*, 4516.
(39) Cox, R. T.; Block, D.; Herve, A.; Picard, R.; Santier, C.; Helbig, R. *Solid State Commun.* **1978**, *25*, 77.
(40) Lane, P. A.; Wei, X.; Vardeny, Z. V. *Phys. Rev. B*, in press.
(41) Swanson, L. S.; Lane, P. A.; Shinar, J. *Phys. Rev. B* **1991**, *44*, 10617.